Journal of Materials Chemistry C

Accepted Manuscript

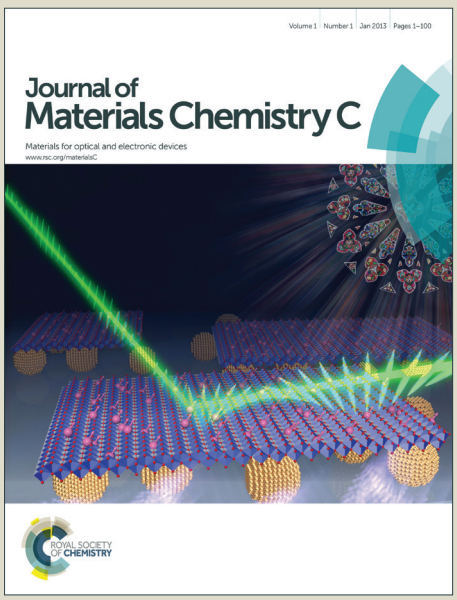

ROYAL SOCIETY OF CHEMISTRY

www.rsc.org/materialsC

Revised Manuscript

Dual-Mode Waveguiding of Raman and Luminescence Signals in a Crystalline Organic Microplate

Seong Gi Jo[a†], *Dong Hyuk Park*[b,c†], *Bong-Gi Kim*[b†], *Sungbaek Seo*[b], *Suk Joong Lee*[d], *Jeongyong Kim*[e*], *Jinsang Kim*[b*], *and Jinsoo Joo*[a*]

[a]Department of Physics, Korea University, Seoul 136-713, Republic of Korea

[b]Materials Science and Engineering, Macromolecular Science and Engineering, University of Michigan, Ann Arbor, Michigan 48109, USA

[c]Division of Nano-systems Engineering, Department of Applied Organic Materials Engineering, Inha University, Incheon 402-751, Republic of Korea

[d]Department of Chemistry, Korea University, Seoul 136-713, Republic of Korea

[e]Center for Integrated Nanostructure Physics (CINAP), Institute of Basic Science (IBS); Department of Energy Science, Sungkyunkwan University, Suwon 440-746, Republic of Korea

† All authors contributed equally to this work.

*Corresponding authors. E-mail: jjoo@korea.ac.kr (J. Joo); Fax: +82-2-927-3292; Tel: +82-2-3290-3103

E-mail: jinsang@umich.edu (Jinsang Kim)

E-mail: j.kim@skku.edu (Jeongyong Kim)

Abstract

We demonstrate dual-mode waveguiding of Raman and luminescence signals using π-conjugated organic 1,4-bis(3,5-bis(trifluoromethyl) cyanostyryl)-2,5-dibromobenzene (CN-TSDB) microplates with single-crystal structure. The output Raman and photoluminescence (PL) spectra through the CN-TSDB microplates were measured as a function of propagation distance using a high-resolution laser confocal microscope (LCM). Under 633 nm Raman excitation, which is outside the optical absorption of the microplates, the characteristic Raman modes of C–Br, $–CF_3$, and –C=C– aromatic stretching were clearly observed at the output points. The decay characteristics of the LCM Raman intensities were comparable to those of LCM PL intensities. The intermolecular π-π interaction of CN-TSDB has been enhanced by the attractive interaction between the CN group and Br atoms, which induces efficient polariton propagation and plays an important role for dual-mode waveguiding.

Introduction

Organic-based optoelectronics, plasmonics, and photonics have been widely studied for their applications in flexible displays,[1-5] bio/chemical sensing,[6-8] and optical communication systems.[9-11] In nanophotonics, nanometer-scale optical waveguides have attracted attention because of their potential for miniaturized photonic circuits and optical communication. Low-dimensional nano- or micro-crystals of photoluminescent materials have been conventionally used as active optical waveguides. Accordingly, their output photoluminescence (PL) spectra and decay characteristics of the PL signal have been intensively investigated.[12-13] The input excitation wavelength should be selected to be within the absorption region of such materials and the PL emission should have efficient overlap with the absorption of the materials to achieve PL signal propagation.

In contrast, a Raman waveguide can uniquely provide direct signal transport using specific molecular interaction modes such as vibrational, rotational, and other low-frequency modes in highly crystalline organic nano- or micro-structures.[14-15] Therefore, extending the optical communication range using nano- or micro-structures from the waveguiding of PL signals to the waveguiding of Raman signals is an interesting subject of research. Indeed, Raman waveguides are capable of transporting multiple signals that correspond to various distinguishable molecular orientations and material vibrations, even when the excitation electromagnetic wave is outside the material's optical absorption range.[16] Moreover, the spectral width of the propagating Raman signal is usually much smaller than that of the PL signal, which suggest that significantly more information can be transmitted using Raman waveguiding.

In this study, we demonstrate dual-mode waveguiding for Raman and PL signals using single crystalline π-conjugated organic 1,4-bis(3,5-bis(trifluoromethyl) cyanostyryl)-2,5-dibromobenzene (CN-TSDB) microplates. Characteristic Raman modes such as the –C=C– aromatic, $–CF_3$, and C–Br stretching modes propagated through the organic microplates with different decay constants. The transmission of various characteristic Raman modes through the organic microplate waveguide indicates a new type of active waveguiding with a much narrower spectral resolution than that transmit a PL signal. This suggests that Raman mode waveguides have the potential to be used in nanophotonic systems that require multi-signal and higher-bandwidth transmissions.

Experimental

Preparation of crystalline organic CN-TSDB microplates.

All starting materials were purchased from commercial suppliers (Sigma Aldrich Co. and Fisher Sci. Co.) and used without further purification. 2-(3,5-bis(trifluoromethyl)phenyl)acetonitrile (1 g, 3.95 mmol) and 2,5-dibromobenzene-1,4-dialdehyde (0.57 g, 1.975 mmol) were dissolved in *tert*-butanol (20 ml) and tetrahydrofuran (1 ml). Then, the mixture was heated to 50˚C, and a 1.0 M solution of tetrabutyl ammonium hydroxide (0.395 ml, 10 mol%) was slowly dropped. After stirring for 1 h, the precipitate was collected through filtration and washed with methanol. The CN-TSDB was finally obtained by recrystallization with chloroform after flash column chromatography under a chloroform eluent.[17] H-NMR (400MHz, DMSO) δ 8.25 (ds, 6H), 8.37 (s, 2H), 8.32 (s, 2H), and m/z

EIMS 761.9. The CN-TSDB powder (1 mg) was dissolved in chloroform (1 ml) solvent and heated to 40˚C. The CN-TSDB microplates were formed via self-assembly during storage in a refrigerator for 12 h.

Measurements

The formation and surface morphologies of the CN-TSDB microplates were investigated using a field-emission scanning electron microscope (FE-SEM, Hitachi S-4300) and high-resolution transmission electron microscope (HR-TEM, JEOL JEM-3010). The ultraviolet and visible (UV/Vis) absorption (Agilent 8453) spectra of the samples were measured in solution. Emission spectra were obtained using a Hitachi F-7000 fluorescence spectrophotometer in quartz cells. X-ray diffraction (XRD) data were collected using a Bruker SMART APEX diffractometer equipped with a monochromator for the Mo Kα (λ = 0.71073 Å) incident beam. Each crystal was mounted onto a glass fiber. Charge-coupled device (CCD) data were integrated and scaled using the Bruker-SAINT software package, while the structure was solved and refined using SHEXTL V6.12. For direct luminescent images, the color CCD images of the CN-TSDB microplates were measured using an AVT Marlin F-033C XGA C-mount camera (λ_{ex} = 435 nm). The nanoscale Raman and PL spectra of the microplates, including their output spectra, were measured using a high–resolution laser confocal microscope (LCM) built around an inverted optical microscope (Axiovert 200, Zeiss GmbH).[18-23] The 405 nm line of an unpolarized argon ion laser was used for the LCM PL excitation. It should be noted that this was the shortest-wavelength laser used in our

system. The 633 nm line of a He-Ne gas laser was used for the Raman excitation, which falls outside the optical absorption region of the CN-TSDB microplates. The diameter of focused laser was about 200 nm. It was changed to approximately 300 nm diameter spot when oil lens was used. On the surface of the microplate, the spot size of the laser seemed to be wider due to the luminescence spreading. The laser power density was 30 μW/cm^2 (405 nm, excitation time: 47.5 ms) and 2.5 mW/cm^2 (633 nm, excitation time: 50 s), while the probe had a significantly lower power density to prevent the destruction of the sample structure.

< Figure 1>

Results and discussion

Formation and structural characteristics of CN-TSDB microplates

The waveguiding characteristics of optical signals are closely related to the crystalline structure as well as the refractive index (n) of the material and waveguide dimensions.[24-25] For an efficient optical waveguide operation, highly crystalline, luminescent nano- or micro-structures are preferred because high crystallinity improves the energy transfer. In this study, single crystals of CN-TSDB were synthesized, and their crystalline packing structure was analyzed using single-crystal XRD data. Figure 1a shows the chemical structure of CN-TSDB. A selected area electron diffraction (SAED) and FE-SEM images (Figures 1b and 1c, respectively) showed that the CN-TSDB microplates have a diamond shape and single-crystal structure. We grew CN-TSDB crystalline microplates with dimensions of up to a few tens of

micrometers and thicknesses between 400 and 500 nm. Figure 1d shows color CCD images of luminescent CN-TSDB microplates when they were excited at different positions (λ_{ex} = 405 nm), which are shown as bright blue spots. Brighter blue emissions from the edges was observed owing to self-waveguiding.[26-27] Figure 1e shows the crystal structure and packing diagrams for the CN-TSDB microplates. Figure 1f shows the face-indexed result (with Miller indices) of a real crystal and corresponding orientation of the unit cells. The CN-TSDB microplates have monoclinic structure: (space group $P2_1/c$), a = 20.1093(5) Å, b = 4.67830(10) Å, c = 14.0181(4) Å, β = 95.8770(10)°, V = 1311.85(6) Å^3, Z = 2.

CCDC 989194 contains the supplementary crystallographic data for this paper. These data can be obtained free of charge from the Cambridge Crystallographic Data Centre via www.ccdc.cam.ac.uk/data_request/cif.

< Figure 2>

The crystal structure of a CN-TSDB microplate is also shown in Figure 2 and Table S1 in the Supporting Information (SI). Figure 2 shows crystal-packing diagrams for the CN-TSDB molecules viewed from different perspectives. Table S1 lists the crystal data and structural refinements of the CN-TSDB microplates. We observed that the CN groups (blue) were tightly packed with the Br atoms (red) of the nearest neighbor CN-TSDB molecules. In Figure 2, the blue dotted lines are in the range of the primitive cell, and the red dotted lines are out of the range of the primitive cell. An attractive interaction between the CN groups and

Br atoms on the nearest neighbor CN-TSDB molecules would aid molecular π-π stacking along the *b*-axis (see Figures 1e and 2 as well as Table S1 in SI).[28] Incorporating halogen atoms (F and Br) inside an organic molecule increases the electron density of the molecule owing to the heavy atom effect. In addition, fluoride can induce closer packing of organic molecules owing to its hydrophobic properties. This close-packed structure of the CN-TSDB microplates contributed to an efficient optical signal propagation.

< Figure 3>

Optical characteristics of CN-TSDB

Figure 3a shows the normalized UV/Vis absorption (black curve) and PL (red curve) spectra of CN-TSDB in a chloroform solution. A maximum absorption λ_{max} was observed near 336 nm, which corresponds to the π-π* transition. The λ_{max} of the solution (λ_{ex} = 405 nm) was observed near 431 nm, with a satellite peak near 449 nm. The solution PL spectrum of CN-TSDB slightly overlaps with the absorption spectrum in the region near 400 nm. The LCM PL peak of the crystalline CN-TSDB microplates was observed at 438 nm, which was slightly red-shifted in comparison to the in-solution PL spectrum, as shown in Figure 3a (and Figure S1 in the SI), due to π-conjugated molecular stacking.[8] Figure 3b shows the LCM Raman spectrum (λ_{ex} = 633 nm) of the CN-TSDB microplates with identical excitation and detection positions. Characteristic Raman modes such as the –C=C– aromatic, $-CF_3$, and C–Br stretching modes were detected in the CN-TSDB microplates at 1580 and 1594 cm^{-1}, 1216 cm^{-1}, and 667 and 687 cm^{-1}, respectively.[29] Detailed assignments of the characteristic Raman

peaks are listed in Table 1.

Table 1. Characteristic Raman modes of the CN-TSDB microplate.

Mode	Region (cm^{-1})	Raman shift (cm^{-1})
C–Br	485-750 140-400	593, 618 667, 687
$–CF_3$	1205-1420 1120-1350 680-780	1216, 1262, 1279, 1340 724, 765
–C=C– aromatic	1575-1625 1430-1525	1580, 1594 1455, 1509
Out-of-plane =C–H	650-900	876
In-plane =C–H	990-1290	1000

< Figure 4>

Raman waveguiding characteristics

Figure 4a shows a schematic illustration of the optical waveguiding experimental setup for the CN-TSDB microplate using an LCM system. The input confocal laser (λ_{ex} = 633 nm for Raman signal) was movable, while the detecting position was fixed at the end of the crystal. The excitation laser beam, which was focused by the objective lens, was perpendicularly irradiated on the sample, and the local light signal from a selected location on the sample was collected with the same objective lens. An optical microscope image of the CN-TSDB microplate (Figure 4a) illustrates the directions of movement for the input laser (represented by yellow arrows), which are arbitrarily denoted as the [*A*], [*B*], and [*C*] directions. It should be noted that the 633 nm excitation for the Raman signals is outside the optical absorption range of CN-TSDB (see Figure 3a). Figures 4b, 4c, and 4d show the waveguide-propagated

Raman spectra (i.e., output Raman signals) of the C–Br (667 and 687 cm^{-1}), $–CF_3$ (1216 cm^{-1}), and –C=C– aromatic (1580 and 1594 cm^{-1}) modes, respectively, along the [*B*] direction, with varying propagation distances (indicated by numbers in the insets). We clearly observed the waveguiding of characteristic Raman modes through the CN-TSDB microplate, i.e., the characteristic Raman modes of the CN-TSDB were detected at the end of the microplate during the movement of the input excitation. The waveguide-propagated Raman spectra along the [*A*] and [*C*] directions (Figure S2) were similar to those along the [*B*] direction. Figures 4e, 4f, and 4g show the output LCM Raman intensities of the C–Br, $–CF_3$, and –C=C– aromatic modes, respectively, as a function of propagation distance along the [*A*], [*B*], and [*C*] directions. The LCM Raman intensity decreased with increasing propagation distance. We suggest that all of the characteristic Raman modes propagated to the end of the sample because of the polariton propagation, i.e., coupled phonon-photon transverse waves.[30,31]

< Figure 5>

Using the results shown in Figures 4e-g, the decay constants (α_R's) versus Raman shift were obtained along the [*A*], [*B*], and [*C*] directions for various Raman modes, as shown in Figure 5. The characteristic equation for this decay curve is $I_R = I_{R0}\, exp(-\alpha_R x)$, where I_R is the output LCM Raman intensity, I_{R0} is the proportional constant for the intensity, α_R is the decay constant in μm^{-1}, and x is the propagation distance of the incident light. The α_R's of the C–Br mode (667 cm^{-1}), =C–H out-of-plane mode (876 cm^{-1}), $–CF_3$ mode (1216 cm^{-1}), and –C=C–

aromatic stretching mode (1594 cm^{-1}) along the [*B*] direction were estimated to be approximately 0.079, 0.083, 0.101, and 0.109 μm^{-1}, respectively. For the [*A*] and [*C*] direction, the values of α_R also increased with increasing Raman shift. We clearly observed that the decay constants for all Raman intensities increased with increasing Raman shift, as shown in Figure 5. Similar results were obtained using samples from another batch of CN-TSBD microplates, as shown in Figures S3, S4, and S5, thereby confirming the reproducibility of these results. These results show that each Raman signal propagates differently, which suggests that individual Raman signals can be used independently to transport signals using Raman waveguiding. The energy difference between the $–CF_3$ (1216 cm^{-1}) and –C=C– aromatic stretching (1594 cm^{-1}) modes is only ~300 cm^{-1}, which corresponds to ~12 nm, and is much smaller than the spectral width of most PL signals. The full width at the half maximum of the output LCM PL spectra was greater than 77 nm (obtained from Figure 6). This suggests that a much higher signal transportation bandwidth is possible using active Raman waveguiding.

The decay characteristics of Raman signals were analyzed using the crystal structure. The α_R of the C–Br mode was the smallest, which is desirable for Raman waveguiding, while that of the –C=C– aromatic mode was the largest, indicating rapid decay of the Raman signal. From the crystal packing diagram shown in Figure 2, the intermolecular distance between the Br atoms in the C–Br groups (red marks) is approximately 4.021 Å. However, the intermolecular distance between the C atoms in the phenyl groups, including the –C=C– aromatic mode, is estimated to be 4.678 Å. Therefore, the output Raman signals are related to

the intermolecular distance of the chemical groups that correspond to the Raman modes. The results suggest that the transport of Raman signals occur through the strong coupling of incident photons and various phonons in the well-stacked CN-TSDB molecules. To the best of our knowledge, we are the first to report such waveguiding of Raman signals using crystalline organic microstructures.

< Figure 6>

PL waveguiding characteristics

We also investigated the PL waveguiding characteristics of the CN-TSDB microplates. The output LCM PL spectra were measured along the [*A*], [*B*], and [*C*] directions at various propagation distances. The input confocal laser (λ_{ex} = 405 nm, which was inside the optical absorption range of the material) was oriented perpendicular to the CN-TSDB microplates. The LCM PL intensity of the waveguide-propagated emissions decreased with increasing propagation distances, as shown in Figure 6. The PL waveguiding characteristics were also analyzed in terms of the decay constant (α_{PL}), using $I_{PL} = I_0 \, exp(-\alpha_{PL} x)$. The values of α_{PL} along the [*A*], [*B*], and [*C*] directions were estimated to be approximately 0.141, 0.102, and 0.071 μm^{-1}, respectively. The absolute values of α_{PL} are comparable to the α_R's for the Raman waveguiding. We also confirmed that the output PL signals were due to the intrinsic waveguiding, not scattered light (not shown in here). Therefore, we successfully observed dual-mode optical waveguiding of Raman and PL signals inside CN-TSDB microplates.

There are several different approaches to optical waveguiding such as using dielectric slab waveguides, optical fibers, and two-dimensional waveguides. Each of these methods are based on refraction and reflection with respect to boundary conditions.[12,13,32] The novel features of this study are the waveguiding of various characteristic Raman modes through the single crystalline CN-TSDB microplates. Waveguiding of Raman signals was successfully performed using a 633 nm excitation laser, whose wavelength was outside the optical absorption range of the material.

Conclusion

In this study, single crystalline CN-TSDB microplates with thicknesses between 400 and 500 nm were fabricated using a self-growth method. Dual-mode optical waveguiding performance of Raman and PL signals was observed for excitation wavelengths of 633 and 405 nm, respectively. Characteristic Raman modes such as C–Br, $–CF_3$, and –C=C– aromatic stretching in the CN-TSDB microplates were observed at the output points, which demonstrates a successful Raman waveguiding. The decay constants of the LCM Raman intensities were comparable with those of the LCM PL intensities. The attractive interaction between the CN groups and Br atoms as well as heavy atoms and hydrophobic effects due to fluoride can induce a close-packed structure, which results in efficient dual-mode optical waveguiding. The Raman waveguiding with a relatively narrower bandwidth, which was demonstrated in this study, can be used for multi-signal transport in the fields of nanophotonics and optical communications.

Acknowledgments

This study was supported by the National Research Foundation (NRF) of Korea, funded by the Ministry of Science, ICT & Future Planning (MSIP) (No. 2012R1A2A2A01045102). Jinsang Kim acknowledges the postdoctoral fellowship for Dr. D.H. Park from World Class University program through NRF (R31-2008-000-10075-0). Jeongyong Kim acknowledges financial support from the Institute for Basic Science (IBS) (EM 1304) in Korea.

Supporting information

See the supporting information section for additional experimental data, including XRD data and optical properties of additional samples.

Notes and References

1. Z. B. Wang, M. G. Helander, J. Qiu, D. P. Puzzo, M. T. Greiner, Z. M. Hudson, S. Wang, Z. W. Liu, Z. H. Lu, *Nature Photon.* 2011, **5**, 753.
2. T. -H. Kim, K. -S. Cho, E. K. Lee, S. J. Lee, J. Chae, J. W. Kim, D. H. Kim, J. -Y. Kwon, G. Amaratunga, S. Y. Lee, B. L. Choi, Y. Kuk, J. M. Kim. K. Kim, *Nature Photon.* 2011, **5**, 176.
3. B. Crone, A. Dodabalapur, Y. -Y. Lin, R. W. Filas, Z. Bao, A. LaDuca, R. Sarpeshkar, H. E. Katz, W. Li, *Nature* 2000, **403**, 521.
4. R. Li, W. Hu, Y. Liu, D. Zhu, *Acc. Chem. Res.* 2010, **43**, 529-540.
5. A. L. Briseno, S. C. B. Mannsfeld, M. M. Ling, S. Liu, R. J. Tseng, C. Reese, M. E. Roberts, Y. Yang, F. Wudl, Z. Bao, *Nature* 2006, **444**, 913-917.
6. J. T. Mabeck, G. G. Malliaras, *Anal. Bioanal. Chem.* 2006, **384**, 343.
7. P. Alivisatos, *Nat. Biotechnol.* 2004, **22**, 47.
8. M. S. Mannoor, H. Tao, J. D. Clayton, A. Sengupta, D. L. Kaplan, R. R. Naik, N. Verma, F. G. Omenetto, M. C. McAlpine, *Nat. Commun.* 2012, **3**, 763.
9. Y. Zhu, X. Hu, Y. Fu, H. Yang, Q. Gong, *Sci. Rep.* 2013, **3**, 2338.
10. A. Jamshidi, P. J. Pauzauskie, P. J. Schuck, A. T. Ohta, P. –Y. Chiou, J. Chou, P. Yang, M. C. Wu, *Nature Photon.* 2008, **2**, 85.
11. R. Yan, D. Gargas, P. Yang, *Nature Photon.* 2009, **3**, 569.
12. L. Heng, X. Wang, D. Tian, J. Zhai, B. Tang, L. Jiang, *Adv. Mater.* 2010, **22**, 4716.
13. Y. S. Zhao, A. Peng, H. Fu, Y. Ma, J. Yao, *Adv. Mater.* 2008, **20**, 1661.

14. D. J. Sirbuly, A. Tao, M. Law, R. Fan, P. Yang, *Adv. Mater*. 2007, **19**, 61.

15. S. Lal, S. Link, N. J. Halas, *Nature Photon*. 2007, **1**, 641.

16. J. Clark, G. Lanzani, *Nature Photon*. 2010, **4**, 438.

17. Z. Xie, B. Yang, L. Liu, M. Li, D. Lin, Y. Ma, G. Cheng, S. Liu, *J. Phys. Org. Chem.* 2005, **18**, 962.

18. Y. S. Zhao, J. Xu, A. Peng, H. Fu, Y. Ma, L. Jiang, J. Yao, *Angew. Chem. Int. Ed.* 2008, **47**, 7301.

19. H. Yu, B. Li, *Sci. Rep.* 2013, **3**, 1674.

20. J. Xu, X. Zhuang, P. Guo, W. Huang, W. Hu, Q. Zhang, Q. Wan, X. Zhu, Z. Yang, L. Tong, X. Duan, A. Pan, *Sci. Rep.* 2012, **2**, 820.

21. D. H. Park, M. S. Kim, J. Joo, *Chem. Soc. Rev*. 2010, **39**, 2439.

22. Y. K. Hong, D. H. Park, S. G. Jo, M. H. Koo, D. -C. Kim, J. Kim, J. -S. Kim, S. -Y. Jang, J. Joo, *Angew. Chem. Int. Ed.* 2011, **50**, 3734.

23. D. H. Park, Y. K. Hong, E. H. Cho, M. S. Kim, D. -C. Kim, J. Bang, J. Kim, J. Joo, *ACS Nano* 2010, **4**, 5155.

24. B. Yan, L. Liao, Y. You, X. Xu, Z. Zheng, Z. Shen, J. Ma, L. Tong, T. Yu, *Adv. Mater.* 2009, **21**, 2436.

25. X. Yan, J. Li, H. Möhwald, *Adv. Mater.* 2011, **23**, 2796.

26. S. Z. Bisri, T. Takenobu, Y. Yomogida, H. Shimotani, T. Yamao, S. Hotta, Y. Iwasa, *Adv. Funct. Mater.* 2009, **19**, 1728.

27. S. Tavazzi, L. Miozzo, L. Silvestri, S. Mora, P. Spearman, M. Moret, S. Rizzato, D. Braga, A. K. D. Diaw, D. Gningue-Sall, J. -J. Aaron, A. Yassar, *Cryst. Growth Des.* 2010, **10**, 2342.

28. B. -K. An, S. H. Gihm, J. W. Chung, C. R. Park, S. -K. Kwon, S. Y. Park, *J. Am. Chem. Soc*. 2009, **131**, 3950.

29. G. Socrates, Infrared and Raman characteristic group frequencies: tables and charts, 3rd Ed, John Wiley & Sons, New York, 2001.

30. K. Takazawa, J. Inoue, K. Mitsuishi, T. Takamasu, *Phys. Rev. Lett.* 2010, **105**, 067401.

31. D. G. Lidzey, D. D. C. Bradley, M. S. Skolnick, T. Virgili, S. Walker, D. M. Whittaker, *Nature* 1998, **395**, 53.

32. S. -G. Jo, S. Kim, E. H. Cho, D. H. Lee, J. Kim, S. J. Lee, J. Joo, *Chem. Asian J*. 2012, **7**, 2768.

Figure Captions

Figure 1. (a) Chemical structure schematic of a CN-TSDB molecule. (b) SAED pattern of a CN-TSDB microplate. (c) SEM image of a CN-TSDB microplate. (d) Color CCD images showing the luminescence of PL waveguides for various CN-TSDB microplates at various excitation positions. (e) Crystal packing diagram for a CN-TSDB microplate. (f) Microscope image and crystal lattice (with Miller indices) for a CN-TSDB microplate.

Figure 2. Crystal packing diagrams for a CN-TSDB microplate viewed from different directions.

Figure 3. (a) Normalized UV/Vis absorbance (black curve) and PL (red curve) spectra of CN-TSDB in a chloroform solution. LCM PL spectrum (blue curve) of a solid CN-TSDB microplate (λ_{ex} = 405 nm). (b) LCM Raman spectrum of a CN-TSDB microplate (λ_{ex} = 633 nm).

Figure 4. (a) Schematic illustration of the optical (Raman and PL) waveguide apparatus using an LCM system. Right: Optical microscope image of a CN-TSDB microplate with the moving directions of an input laser represented by yellow arrows. Variation of waveguided LCM Raman spectra (λ_{ex} = 633 nm) of the (b) C–Br, (c) –CF_3, and (d) –C=C– aromatic stretching modes along the [*B*] direction. LCM Raman intensity of the (e) C–Br mode (667 and 687 cm^{-1}), (f) –CF_3 mode (1216 cm^{-1}), and (g) –C=C– aromatic (1580 and 1594 cm^{-1}) stretching modes versus propagation distance along the [*A*], [*B*], and [*C*] directions.

Figure 5. Plot of the decay constants (μm^{-1}) of the Raman intensity versus Raman shift (cm^{-1}) along the [*A*], [*B*], and [*C*] directions for the characteristic Raman modes: C–Br mode between 667 and 687 cm^{-1}, =C–H out-of-plane mode at 876 cm^{-1}, –CF_3 mode at 1216 cm^{-1}, and –C=C– aromatic mode at 1594 cm^{-1}.

Figure 6. Output LCM PL spectra (λ_{ex} = 405 nm) of waveguided emissions along the (a) [*A*], (b) [*B*], and (c) [*C*] directions. (d) Output LCM PL intensity versus propagation distance along the [*A*], [*B*], and [*C*] directions.

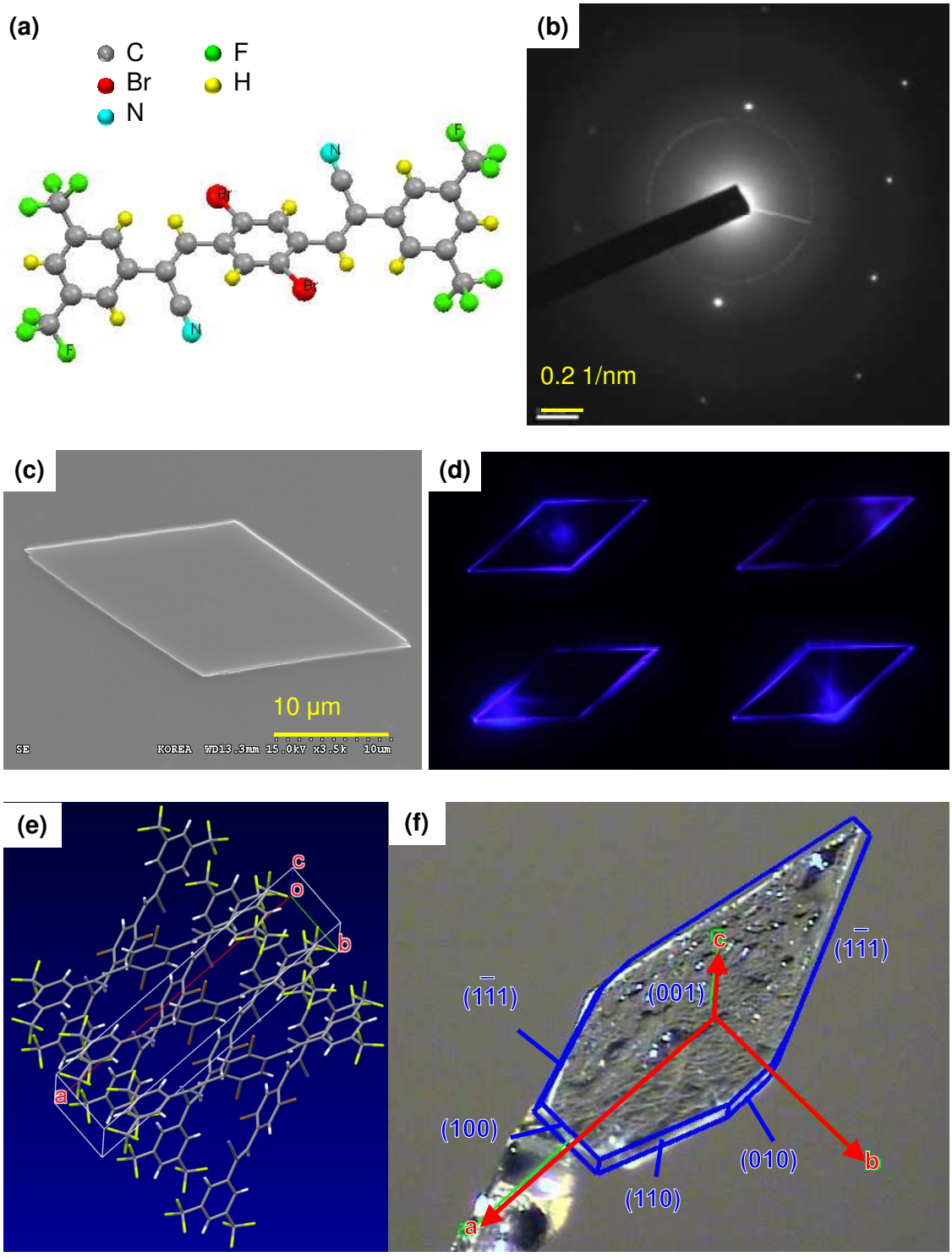

Figure 1

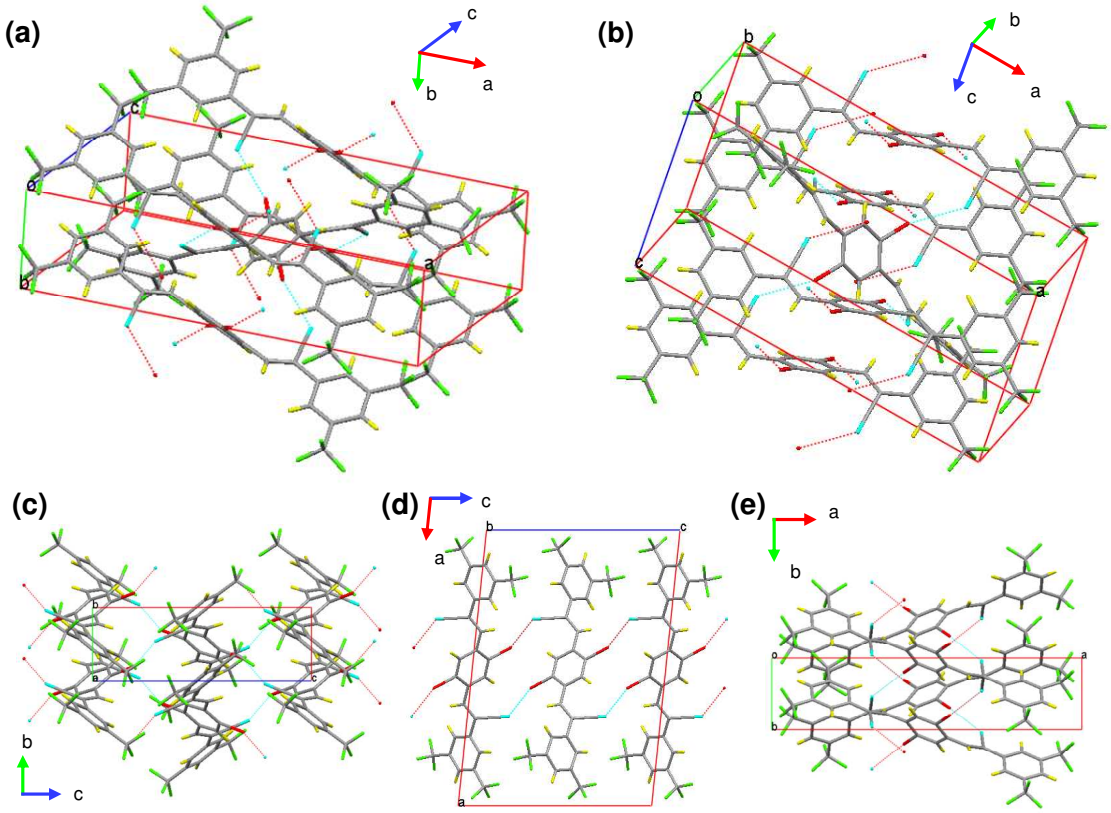

Figure 2

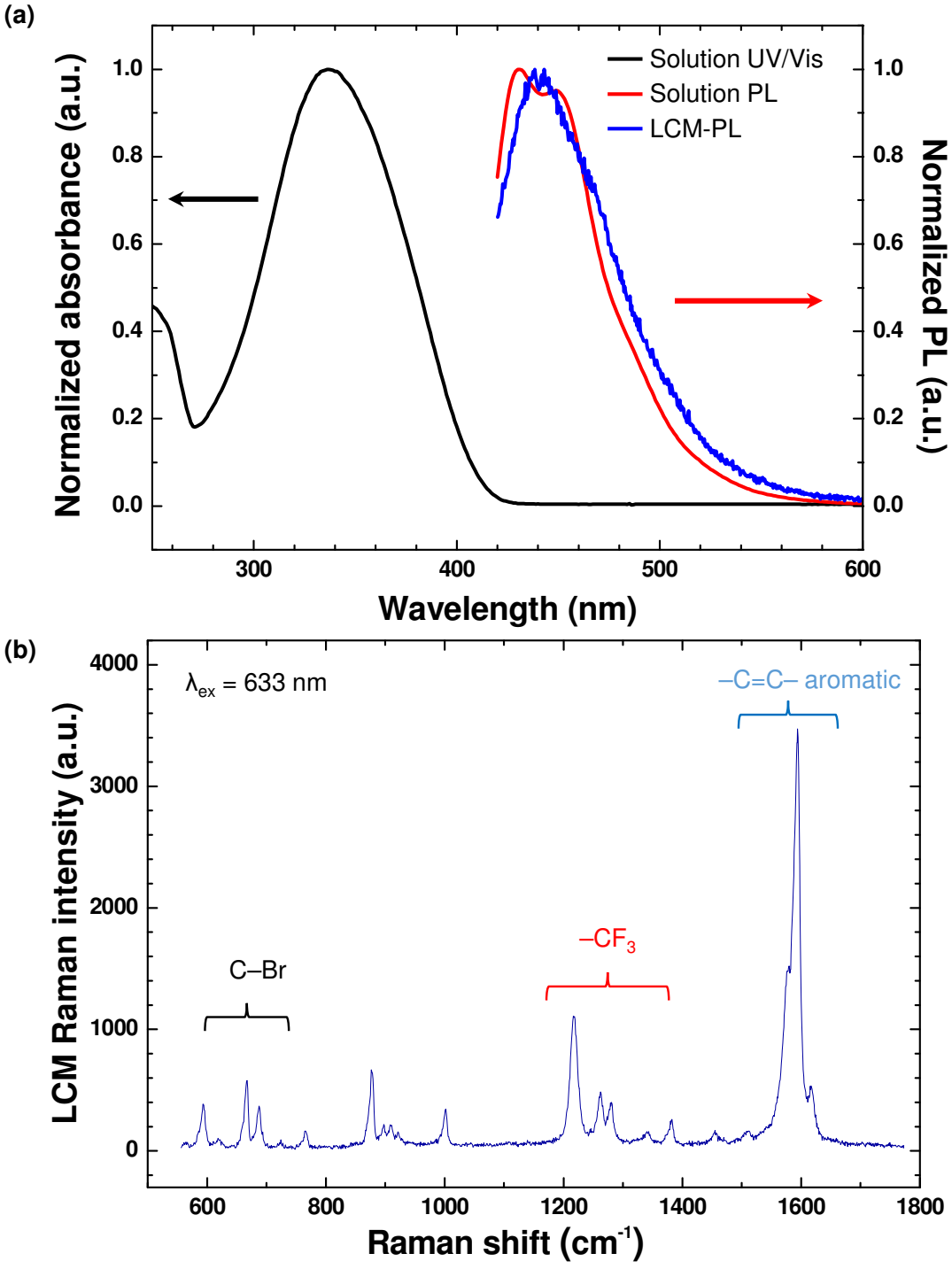

Figure 3

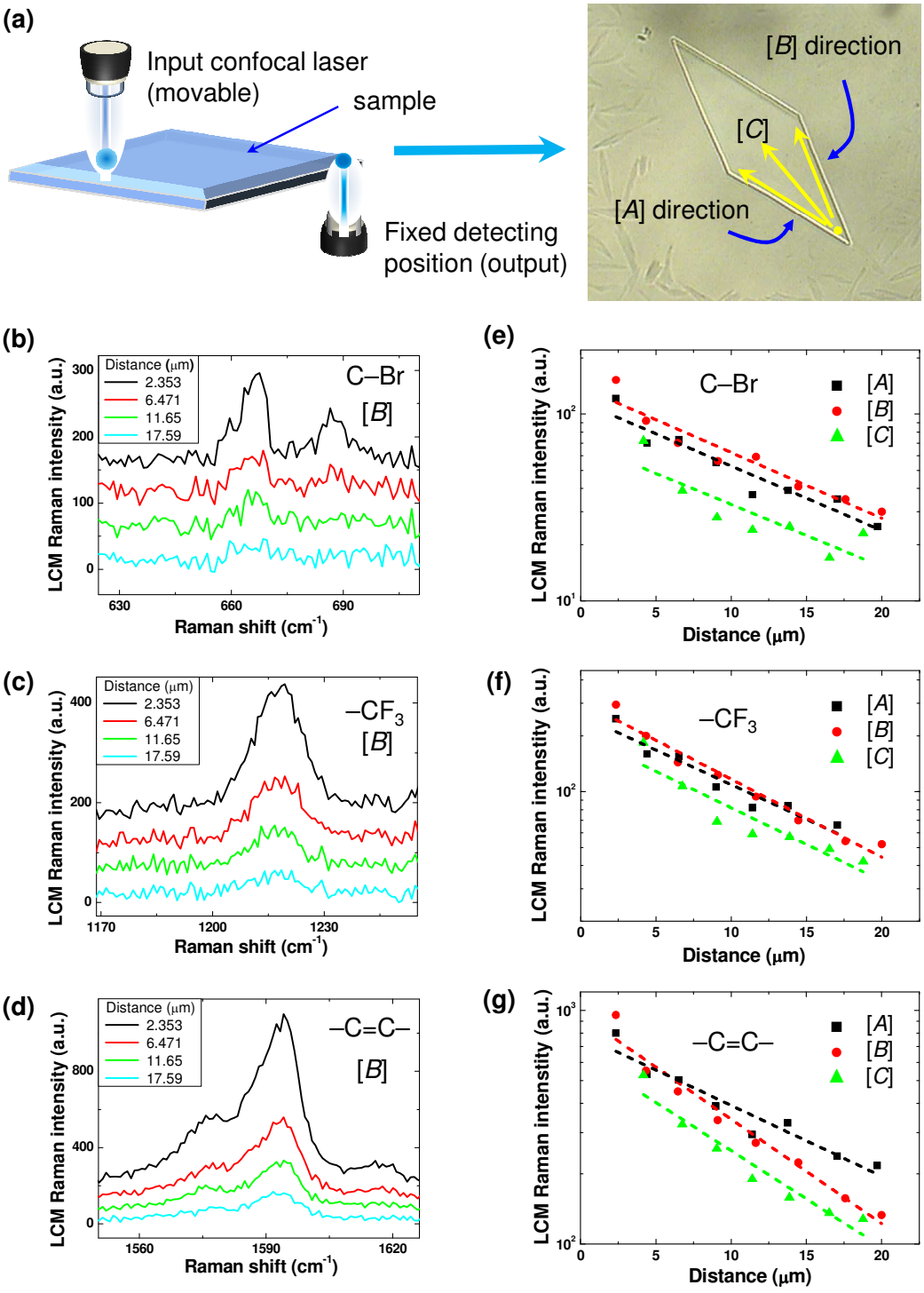

Figure 4

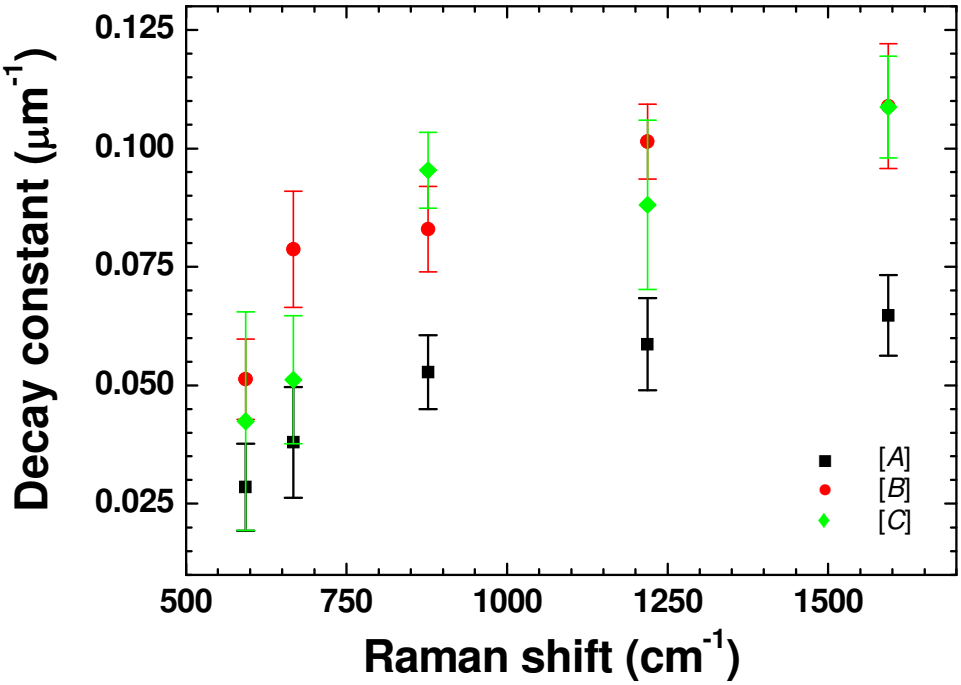

Figure 5

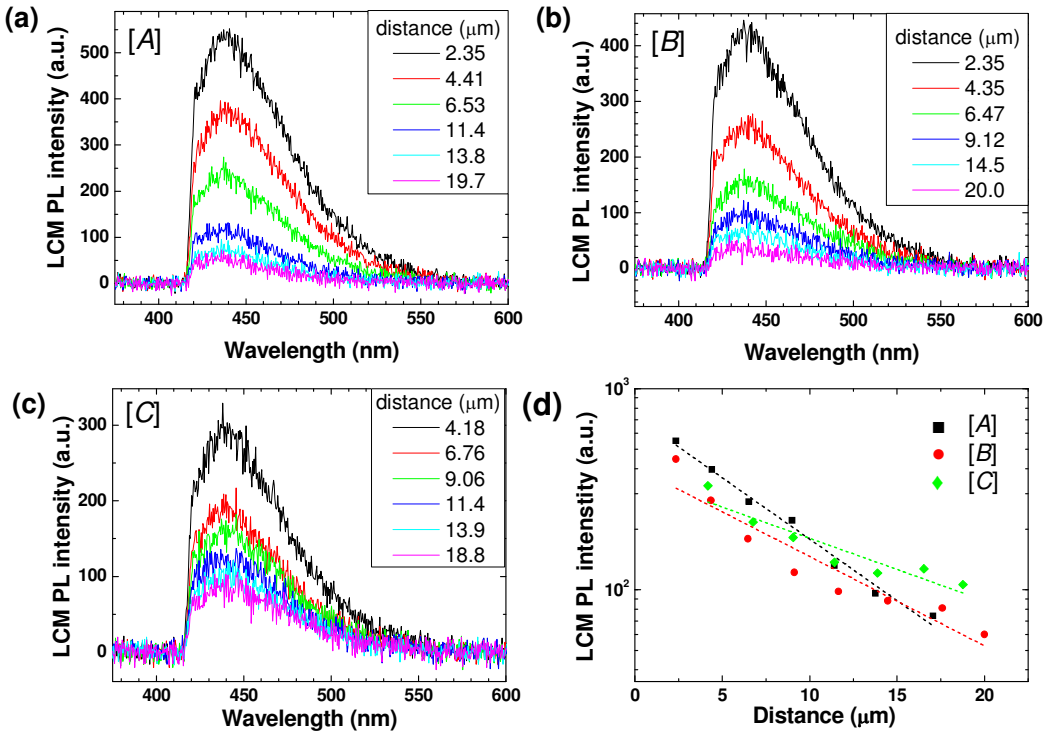

Figure 6